STRUCTURAL BIOLOGY COMMUNICATIONS

ISSN 2053-230X

Sleuthing biochemical evidence to elucidate unassigned electron density in a CBL–SLAP2 crystal complex

Leanne E. Wybenga-Groot[a]* and C. Jane McGlade[b]

[a]SPARC BioCentre, The Hospital for Sick Children, 686 Bay Street, Toronto, Ontario M5G 0A4, Canada, and [b]Program in Cell Biology, The Hospital for Sick Children, 686 Bay Street, Toronto, Ontario M5G 0A4, Canada. *Correspondence e-mail: leanne.wybenga-groot@sickkids.ca

Received 8 October 2020
Accepted 26 January 2021

Edited by S. Sheriff, Bristol-Myers Squibb, USA

Keywords: unknown unassigned electron density; protein–protein interaction; feature-enhanced map; E3 ubiquitin ligase; adaptor proteins; mass spectrometry.

PDB reference: CBL–SLAP2 complex, 6xar

Supporting information: this article has supporting information at journals.iucr.org/f

The Src-like adaptor proteins (SLAP/SLAP2) bind to CBL E3 ubiquitin ligase to downregulate antigen, cytokine and tyrosine kinase receptor signalling. In contrast to the phosphotyrosine-dependent binding of CBL substrates through its tyrosine kinase-binding domain (TKBD), CBL TKBD associates with the C-terminal tail of SLAP2 in a phospho-independent manner. To understand the distinct nature of this interaction, a purification protocol for SLAP2 in complex with CBL TKBD was established and the complex was crystallized. However, determination of the complex crystal structure was hindered by the apparent degradation of SLAP2 during the crystallization process, such that only the CBL TKBD residues could initially be modelled. Close examination of the CBL TKBD structure revealed a unique dimer interface that included two short segments of electron density of unknown origin. To elucidate which residues of SLAP2 to model into this unassigned density, a co-expression system was generated to test SLAP2 deletion mutants and define the minimal SLAP2 binding region. SLAP2 degradation products were also analysed by mass spectrometry. The model-building and map-generation features of the *Phenix* software package were employed, leading to successful modelling of the C-terminal tail of SLAP2 into the unassigned electron-density segments.

1. Introduction

The amino-terminal tyrosine kinase-binding domain (TKBD) of CBL E3 ubiquitin ligase consists of a four-helix bundle (4H), an EF-hand and a variant SH2 domain. The variant SH2 domain binds CBL substrates, such as phosphorylated tyrosine kinases, in a canonical phosphotyrosine-dependent manner (Meng *et al.*, 1999). CBL TKBD also binds Src-like adaptor proteins (SLAP and SLAP2), and this interaction is important for the regulation of antigen, cytokine and tyrosine kinase (TK) signalling by CBL (Sosinowski *et al.*, 2000, 2001; Loreto & McGlade, 2003; Loreto *et al.*, 2002; Myers *et al.*, 2006; Dragone *et al.*, 2006, 2009; Naramura *et al.*, 1998; Lebigot *et al.*, 2003; Pakuts *et al.*, 2007). SLAP2 is composed of adjacent SH3 and SH2 domains that are most closely related to those found in the SRC family kinase HCK, followed by a carboxy-terminal tail region that is void of apparent domains or protein–protein interaction motifs and is predicted to be predominantly disordered (Pandey *et al.*, 1995; Tang *et al.*, 1999; Wybenga-Groot & McGlade, 2013, 2015; Loreto *et al.*, 2002). While the SLAP2 SH3/SH2 domains mediate binding to activated receptor TKs, the C-terminal tail region of SLAP2 associates with CBL TKBD in a phosphotyrosine-independent manner (Loreto & McGlade, 2003; Holland *et al.*, 2001; Myers *et al.*, 2006), suggesting that the interaction between CBL and SLAP2 is distinct and is likely to represent a novel mode of

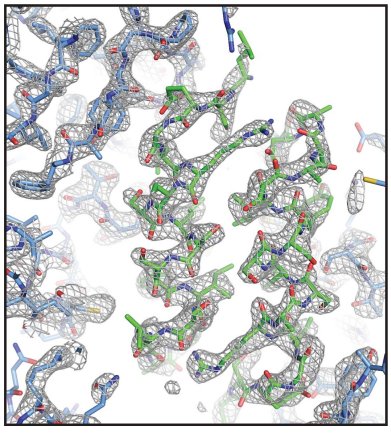

Table 1
Macromolecule-production information.

	GST-CBL 25–357	(Trx)-His_6-mSLAP2 28–259
Source organism	*Homo sapiens*	*Mus musculus*
Forward primer†	GGATCTGGTTCCGCGTGGATCCCTGATTGGGCTCATGAAGGACG	GGAAGATCTCAACCAGAAAGACACAAGGTC
Reverse primer‡	CGTCCTTCATGAGCCCAATCAGGGATCCACGCGGAACCAGATCC	CCGCTCGAGCTAAGCATCATCCAAGGG
Cloning vector	pGEX-4T-1	pGEX-4T-1
Expression vector	pGEX-4T-1	pET32a-mod
Expression host	*E. coli* strain BL21	*E. coli* strain BL21
Complete amino-acid sequence of the construct produced§	(GS)LIGLMKDAFQPHHHHHHHHLSPHPPGTVDKKMVEKCWKLMDKVVRLCQNPKLALKNSPPYILDLLPDTYQHLRTILSRYEGKMETLGENEYFRVFMENLMKKTKQTISLFKEGKERMYEENSQPRRNLTKLSLIFSHMLAELKGIFPSGLFQGDTFRITKADAAEFWRKAFGEKTIVPWKSFRQALHEVHPISSGLEAMALKSTIDLTCNDYISVFEFDIFTRLFQPWSSLLRNWNSLAVTHPGYMAFLTYDEVKARLQKFIHKPGSYIFRLSCTRLGQWAIGYVTADGNILQTIPHNKPLFQALIDGFREGFYLFPDGRNQNPDLTGLCEPTP	(GS)QPERRKVTAVALGSFPAGEQARLSLRLGEPLTIISEDGDWWTVQSEVSGREYHMPSVYVAKVAHGWLYEGLSREKAEELLLLPGNPGGAFLIRESQTRRGCYSLSVRLSRPASWDRIRHYRIQRLDNGWLYISPRLTFPSLHALVEHYSELADGICCPLREPCVLQKLGPLPGKDTPPPVTVPTSSLNWKKLDRSLLFLEAPASGEASLLSEGLRESLSSYISLAEDPLDDA

† The BglII site is underlined. ‡ The XhoI site is underlined. § After thrombin cleavage, GS residues from the thrombin cleavage site remain.

binding. Indeed, binding of SLAP2 to CBL is not disrupted by a Gly306Glu mutation in CBL, which abolishes the binding of TKBD to tyrosine-phosphorylated substrates (Loreto *et al.*, 2002). To understand the molecular basis of this interaction, we purified and crystallized CBL TKBD in complex with SLAP2. Initial efforts to determine the structure of the CBL–SLAP2 complex resulted in the structure of a CBL dimer with two unassigned regions of electron density nestled in the dimer interface that resembled α-helices. This paper describes how we used biochemical and mass-spectrometric techniques to determine which residues of SLAP2 to model into this unknown, unassigned electron density.

2. Materials and methods

2.1. Macromolecule production

For co-crystallization experiments, residues 2–25 were deleted from human glutathione-*S*-transferase (GST)-CBL 2–357 using standard QuikChange methods to generate human GST-CBL 25–357. Residues 28–259 of mouse SLAP2 (mSLAP2) were cloned in-frame into a modified pET-32a (pET3-2a-mod) vector (with a TEV cleavage site downstream of the His tag and 17 residues upstream of the thrombin cleavage site; a gift from Gil Privé's laboratory, University Health Network) with BamHI/BglII and XhoI sites to express thioredoxin (Trx)-His_6-mSLAP2 28–259. Cloning information is summarized in Table 1.

Trx-His_6-mSLAP2 was transformed into *Escherichia coli* BL21 cells and grown in 8 l Luria–Bertani (LB) medium supplemented with 50 µg ml^{-1} ampicillin (Amp) overnight at 289 K [A_{600} = 0.6–0.9; induction with 0.5 m*M* isopropyl β-D-1-thiogalactopyranoside (IPTG)]. The cells were collected by centrifugation, and the cell pellet was frozen at 193 K, thawed, resuspended in 150 ml lysis buffer [50 m*M* HEPES pH 7.5, 0.5 *M* NaCl, 10% glycerol, 10 m*M* imidazole, 10 m*M* β-mercaptoethanol (βME), 10 m*M* $MgCl_2$, 5 m*M* $CaCl_2$, cOmplete EDTA-free protease-inhibitor cocktail tablets (inhibitor tablets; Roche Applied Science), Benzonase nuclease, 1 m*M* phenylmethylsulfonyl fluoride (PMSF)] and lysed by three cycles of high-pressure homogenization (Emulsiflex) and two cycles of sonication on ice. Following centrifugation, the supernatant was mixed with Ni–NTA agarose (Qiagen) for 90 min by gentle nutation at 277 K. The resin was washed with 6 × 25 ml wash buffer (50 m*M* HEPES pH 7.5, 0.5 *M* NaCl, 10% glycerol, 20 m*M* imidazole, 10 m*M* βME, 10 m*M* $MgCl_2$, 5 m*M* $CaCl_2$) and SLAP2 was eluted with wash buffer containing increasing concentrations of imidazole (75, 150, 225 and 300 m*M* imidazole, 28 ml total elution volume). The Trx-His_6 tag was cleaved by the addition of 300 units of thrombin (Sigma, catalogue No. T4648) directly to the eluate and the solution was dialyzed (Slide-A-Lyzer dialysis cassettes, Thermo Scientific, 3500 molecular-weight cutoff) overnight at room temperature (RT) against 2 l dialysis buffer (25 m*M* HEPES pH 7.5, 0.4 *M* NaCl, 4% glycerol, 10 m*M* imidazole, 5 m*M* βME, 5 m*M* $MgCl_2$, 5 m*M* $CaCl_2$). The solution was removed from the dialysis cassette and centrifuged at 4000 rev min^{-1} for 7 min to remove precipitate, and PMSF was added to the soluble portion to 1 m*M*. This SLAP2 solution was passed very slowly over the same aliquot of Ni–NTA resin (washed since elution) to remove Trx-His_6, concentrated with a centrifugal filter unit (Amicon Ultra, Millipore) and flash-frozen in liquid nitrogen for storage at 193 K.

To express CBL TKBD, GST-CBL was overexpressed and the cells were harvested as above (except that expression took place for 6.5 h at 310 K with 1 m*M* IPTG). The cell pellet was resuspended in 100 ml lysis buffer (50 m*M* HEPES pH 7.5, 0.5 *M* NaCl, 10% glycerol, 10 m*M* βME, 2 m*M* $MgSO_4$, inhibitor tablets and Benzonase nuclease) and lysed as above. Following centrifugation, the supernatant was mixed with Glutathione Sepharose 4B (GE Healthcare) for 90 min by gentle nutation at 277 K. The resin was washed with 6 × 25 ml wash buffer (50 m*M* HEPES pH 7.5, 0.5 *M* NaCl, 10% glycerol, 10 m*M* βME, 5 m*M* $CaCl_2$). Thrombin (150 units) was then added directly to the resin and left overnight at

Table 2
Macromolecule-production information for co-purification experiments.

Construct name	Expression vector	Contents
Trx-His$_6$-hSLAP2	pET32a-mod	Trx, TEV site, thrombin site, SLAP2 29–261
Trx-His$_6$-Δlinker-hSLAP2	pET32a-mod	Trx, TEV site, thrombin site, SLAP2 29–261
Duet-His-hSLAP2-CBL	pETDuet-1	Trx, TEV site, thrombin site, SLAP2 29–261 in MCS1; CBL 47–357 in MCS2
Duet-His-hSLAP2-CBL 29–261 Δ198–229	pETDuet-1	Trx, TEV site, thrombin site, SLAP2 29–197 and 230–261 in MCS1; CBL 47–357 in MCS2
Duet-His-hSLAP2-CBL 29–254 Δ198–229	pETDuet-1	Trx, TEV site, thrombin site, SLAP2 29–197 and 230–254 in MCS1; CBL 47–357 in MCS2
Duet-His-Δlinker-hSLAP2-CBL 261	pETDuet-1	Trx, TEV site, SLAP2 29–261 in MCS1; CBL 47–357 in MCS2
Duet-His-Δlinker-hSLAP2-CBL 254	pETDuet-1	Trx, TEV site, SLAP2 29–254 in MCS1; CBL 47–357 in MCS2

277 K; thrombin addition and incubation were repeated at RT. CBL was eluted by washing the resin with elution buffer (25 m*M* HEPES pH 7.5, 0.4 *M* NaCl, 5% glycerol, 5 m*M* βME), concentrated as above and stored stably at 277 K for several weeks.

Approximately 33 mg CBL or 10 mg mSLAP2 were loaded individually onto a HiLoad 16/60 Superdex 75 gel-filtration column (GE Healthcare Life Sciences) equilibrated with GF buffer (25 m*M* HEPES pH 7.5, 0.4 *M* NaCl, 2% glycerol, 5 m*M* βME) and protein elution was detected by monitoring A_{280}. Fractions corresponding to isolated CBL or SLAP2 were assessed for purity by 12.5% SDS–PAGE analysis. To isolate the CBL–SLAP2 complex, purified CBL and SLAP2 were mixed in a 1:1 molar ratio, concentrated to 1 ml and loaded onto the same gel-filtration column as above. Fractions corresponding to the co-elution of CBL and SLAP2 were assessed for purity by 12.5% SDS–PAGE analysis and were concentrated to 11.2 mg ml^{-1}. [The concentration was estimated by measuring the absorbance of the protein at 280 nm and calculating its concentration using a combined CBL/SLAP2 molecular extinction coefficient of 94 810 M^{-1} cm^{-1} as predicted by *ProtParam* (http://web.expasy.org; Gasteiger *et al.*, 2003).]

For the generation of co-expression constructs, residues 29–261 of human SLAP2 (hSLAP2) were cloned in-frame into pET-32a-mod vector with BamHI/BglII and XhoI sites to express (Trx)-His$_6$-hSLAP2. (Note: human SLAP2 protein behaved better than mouse SLAP2 in some purification and biochemical experiments. Thus, given their high sequence conservation, human SLAP2 protein was at times investigated instead of mouse SLAP2.) Using standard QuikChange methods, 19 residues downstream of the TEV cleavage site were deleted from Trx-His$_6$-hSLAP2, thus abolishing the thrombin cleavage site and placing the TEV cleavage site in closer proximity to the N-terminus of the protein, to generate Trx-His$_6$-Δlinker-hSLAP2. Trx-His$_6$-hSLAP2 or Trx-His$_6$-Δlinker-hSLAP2 were cloned in-frame into multiple cloning site 1 (MCS1) of pETDuet-1 (Novagen), with CBL (47–357) cloned in-frame into MCS2 of the same pETDuet-1 vector, for the co-expression of SLAP2 and CBL (Duet-His-hSLAP2-CBL and Duet-His-Δlinker-hSLAP2-CBL 261). Standard QuikChange site-directed mutagenesis methods were employed to delete residues 255–261 of SLAP2 in Duet-His-Δlinker-hSLAP2-CBL 254 and to delete residues 198–229 and 255–261 in Duet-His-hSLAP2-CBL 29–261 Δ198–229 and 29–254 Δ198–229. Construct information is summarized in Table 2.

For the co-expression of CBL and SLAP2, Duet-His-hSLAP2-CBL, Duet-His-Δlinker-hSLAP2-CBL 261 and 254 and the truncation constructs Duet-His-hSLAP2-CBL 29–261 Δ198–229 and 29–254 Δ198–229 were overexpressed in *E. coli* BL21 cells (100 ml LB, 50 µg ml^{-1} Amp, overnight growth at 289–291 K and induction with 0.35–0.5 m*M* IPTG). The cell pellets were resuspended in SLAP2 lysis buffer as above (but with 25 m*M* HEPES pH 7.5 and 150 m*M* NaCl), lysed by sonication and purified as above on Ni–NTA agarose (Qiagen) with wash buffer (25 m*M* HEPES pH 7.5, 150 m*M* NaCl, 2% glycerol, 20 m*M* imidazole, 10 m*M* βME). For the isolation of CBL and SLAP2 in complex from Duet-His-hSLAP2-CBL, the protein was processed as above for SLAP2 (except that 25 m*M* HEPES pH 7.5, 0.4 *M* NaCl, 5% glycerol, 10 m*M* βME, 5 m*M* $CaCl_2$ was used as the dialysis buffer). The CBL–SLAP2 complex was further purified by gel-filtration chromatography and assessed for purity as above with GF buffer (but with 5% glycerol). Alternatively, for analysis of the Ni–NTA-bound complex from the other Duet constructs, the bead slurry was mixed with SDS 2× loading buffer, boiled and analysed by 12.5% SDS–PAGE stained with Coomassie Blue.

2.2. Crystallization of the CBL–SLAP2 complex

Initial crystallization trials of the co-eluted CBL–SLAP2 complex were carried out with commercially available screens (JCSG Core Suites, Qiagen) by the sitting-drop vapour-diffusion method using equal volumes (200 nl) of protein sample (5 mg ml^{-1}) and reservoir solution dispensed using a Mosquito robot (TTP Labtech). Small rod-like crystals were observed after approximately five months in 0.18 *M* HEPES pH 7.5, 10%(*w*/*v*) PEG 8000. A solution of 50% glycerol was added to the drop prior to harvesting and flash-cooling the crystals in liquid nitrogen. Crystallization information is summarized in Table 3.

2.3. Data collection and processing for the CBL–SLAP2 complex

Diffraction data were collected at the Advanced Photon Source and were processed with *QuickScale* (*POINTLESS*, *AIMLESS*/*SCALA*, *CTRUNCATE*) in *MOSFLM* to 2.9 Å resolution (Winn *et al.*, 2011; Evans, 2011). Initial attempts at molecular replacement (MR) were performed with *Phaser_MR* in *Phenix* (Liebschner *et al.*, 2019) using CBL TKBD (PDB entry 2cbl; Meng *et al.*, 1999), one SH3 domain from Lck (PDB entry 1lck; Eck *et al.*, 1994) and one SH2 domain from Lck (PDB entry 1lck) as a model. The same

Table 3
Crystallization.

Method	Sitting-drop vapour diffusion
Plate type	96-well Intelli-Plate
Temperature (K)	293
Protein concentration (mg ml^{-1})	5
Buffer composition of protein solution	25 m*M* HEPES pH 7.5, 0.4 *M* NaCl, 5% glycerol, 5 m*M* βME
Composition of reservoir solution	0.1 *M* HEPES pH 7.5, 10%(*w*/*v*) PEG 8000
Volume and ratio of drop	0.2 µl; 1:1
Volume of reservoir (µl)	75

diffraction data were reprocessed as above to 2.5 Å resolution and subsequent attempts at MR were performed with *Phaser_MR* using CBL TKBD (PDB entry 1b47; Meng *et al.*, 1999) as a model. Anisotropic scaling of the data was performed (http://services.mbi.ucla.edu/anisoscale/) followed by multiple iterative cycles of model building in *Coot* and refinement with *phenix_refine* (Emsley & Cowtan, 2004; Adams *et al.*, 2010; Emsley *et al.*, 2010). A feature-enhanced map (FEM; Afonine *et al.*, 2015) was calculated using *Phenix* and polyglycine chains were placed in the unassigned density of the new FEM using the 'Find Helices and Strands' feature in *Phenix*. Polyglycines were manually converted to polyalanines and then to mSLAP2 residues ^{240}GLRESLSSYI SLAEDP^{255} in both chains of unassigned density. Real-space refinement was performed with *Coot* and refinement with *Phenix*. After calculating a second FEM, residues ^{237}LSE^{239} were assigned. Symmetry-related molecules and superpositions were calculated in *Coot*. Data-collection and processing statistics are summarized in Table 4.

2.4. Mass spectrometry

SDS–PAGE gel bands were reduced, alkylated and digested with trypsin protease as per the in-gel digestion protocol of the SPARC BioCentre at The Hospital for Sick Children (https://lab.research.sickkids.ca/sparc-molecular-analysis/services/mass-spectrometry/mass-spectrometry-sample-protocols/). Digested peptides were subjected to LC-MS/MS at SPARC BioCentre (60 min gradient, Thermo LTQ Orbitrap) and raw data were searched with the *Mascot* and *X!Tandem* software against the human proteome, with carbamidomethylation (C) as a fixed modification and pyroglutamate (Q, N-terminal E), *S*-carbamoylmethylcysteine cyclization (N-terminus), deamidation (NQ), oxidation (M) and acetylation (N-terminus) as variable modifications.

2.5. Isothermal titration calorimetry

Purified CBL TKBD protein and peptides representing the C-terminal tail of mSLAP2 (LSSYISLAEDPLD), the phosphorylated kinase activation loop of Lyn kinase (Lyn-pY; VIEDNEpYTAR) and phosphorylated Zap70 kinase (Zap70-pY; TLNSDGpYTPEPA) were employed in isothermal titration calorimetry (ITC) experiments, which were performed on a VP-ITC Microcalorimeter (MicroCal, Northampton, Massachusetts, USA). CBL TKBD protein and peptide solutions were made in 20 m*M* HEPES pH 7.0, 200 m*M* NaCl and

Table 4
Data collection and processing.

Values in parentheses are for the outer shell.

Diffraction source	24-ID-C, Advanced Photon Source
Wavelength (Å)	0.97921
Temperature (K)	100
Detector	ADSC Quantum 315
Crystal-to-detector distance (mm)	450
Rotation range per image (°)	1
Total rotation range (°)	159
Space group	$P2_1$
a, *b*, *c* (Å)	62.73, 86.96, 65.26
α, β, γ (°)	90, 112.31, 90
Mosaicity (°)	0.54
Resolution range (Å)	45.32–2.50
Total No. of reflections	59065
No. of unique reflections	20374
Completeness (%)	90.5 (57.8)
Multiplicity	2.9 (2.0)
$\langle I/\sigma(I)\rangle$	8.3 (1.5)†
R_{meas} (%)	9.8 (80.6)
Overall *B* factor from Wilson plot (Å^2)	40

† $I/\sigma(I)$ is 2.0 at D_{mid} = 2.66 Å; 2.50 Å was chosen as the resolution limit based on anisotropic scaling of the data.

were degassed just prior to titrations. The reference cell was filled with degassed distilled water. Aliquots of 10 µl SLAP2 or Lyn-pY peptide at 137–155 µ*M* were injected at 3–4 min intervals into the sample cell, which contained CBL at 14 µ*M*. Aliquots of 10 µl Zap70-pY peptide at 223 µ*M* were injected at 5 min intervals with CBL at 21 µ*M* in the sample cell. Titration curves were analysed using the *Origin* software provided by MicroCal.

3. Results and discussion

To understand the molecular basis for the binding of the adaptor protein SLAP2 to CBL TKBD, mouse SLAP2 (residues 28–259) and CBL TKBD (residues 25–357) were purified by affinity and size-exclusion chromatography (Figs. 1*a* and 1*b*). To form a complex of CBL TKBD and SLAP2 for co-crystallization studies, the purified proteins were mixed in a 1:1 molar ratio and subjected to size-exclusion chromatography (Fig. 1*c*). The proteins eluted as two peaks, one at an earlier volume than typically observed for either CBL TKBD or SLAP2, indicating a higher molecular weight (Fig. 1*c*). As confirmed by SDS–PAGE of the chromatographic fractions, the first peak contained a CBL–SLAP2 complex (Fig. 1*d*), which was concentrated and used in sparse-matrix crystallization experiments. Small rod-like crystals (Fig. 1*e*) diffracted to 2.5 Å resolution, albeit with strong anisotropy, at the Advanced Photon Source. After integrating and scaling the diffraction data (Table 4), the Matthews coefficient formula predicted that the asymmetric unit contained one CBL TKBD molecule and one SLAP2 molecule. However, when *Phaser_MR* searched for a solution using one molecule of CBL TKBD (PDB entry 2cbl), one SH3 domain from Lck (PDB entry 1lck) and one SH2 domain from Lck (PDB entry 1lck) as search models (the structure of the SLAP2 SH3/SH2 module had not yet been solved), the translation-function *Z*-score (TFZ) and log-likelihood gain (LLG) were low (TFZ

of 4.2–9.9), indicating a poor MR solution. In contrast, when *Phaser_MR* searched for a solution with two molecules of CBL TKBD, the TFZ score increased to 15.7, suggesting that a correct solution had been found. Limited refinement of the model resulted in an R factor of 0.375 and an R_{free} of 0.424. Examination of crystal packing and symmetry-related molecules suggested insufficient open space for full-length SLAP2 (Figs. 2*a* and 2*b*). Given that the structure of CBL TKBD had already been solved and published numerous times, further refinement of this model was not immediately pursued. However, superposition of the C^{α} atoms of one molecule from our CBL TKBD model with one CBL TKBD molecule from structures available in the Protein Data Bank at the time (for example, PDB entries 3bux, 3buw and 3bum; Ng *et al.*, 2008) revealed a similar mode of configuration or packing of CBL molecules in the published structures and a distinct mode of interaction in our model. In the published structures, interactions between CBL molecules are mediated through the EF-hands (Fig. 2*c*), while the dimer interface in our model involves the EF-hand and 4H bundle (Fig. 2*d*). More importantly, unassigned electron density resembling two α-helices appeared in the space between the two CBL TKBD molecules in our model (Figs. 2*e* and 2*f*). Although the quality of the density and its helical side chains was not sufficient to establish the sequence registry, we reasoned that the density was likely to represent a portion of the SLAP2 protein that co-crystallized with CBL. However, detailed understanding of the structure of SLAP2 and its interaction with CBL, which is required to model the appropriate SLAP2 residues into the density, were not available. It is unlikely that the missing CBL

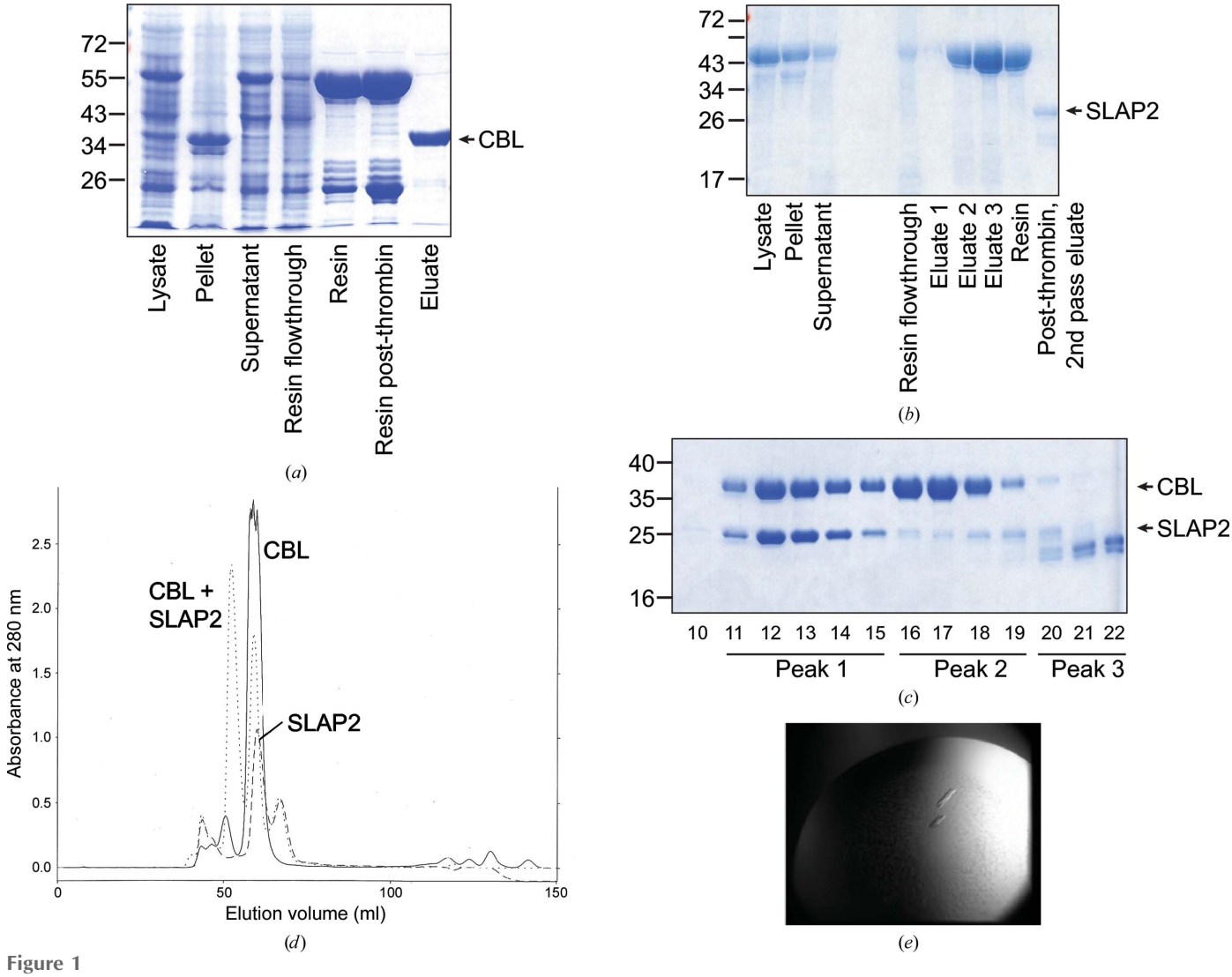

Figure 1
Purification and crystallization of CBL TKBD and SLAP2. (*a*) SDS–PAGE gel stained with Coomassie Blue of samples from stages of CBL TKBD protein purification. (*b*) As in (*a*) for mouse SLAP2. (*c*) Absorbance chromatograms (280 nm) for CBL TKBD (solid line) and mSLAP2 (hatched line) proteins subjected to gel-filtration analysis individually and mixed in a 1:1 molar ratio (dotted line). Comparison of our SEC data for CBL and CBL–SLAP2 with that for standard proteins (chymotrypsinogen A, 25 kDa; carbonic anhydrase, 29 kDa; ovalalbumin, 45 kDa; albumin, 67 kDa; aldolase, 158 kDa) suggests that the major peak for CBL is monomeric and the major peak for the complex is consistent with a 1:1 stoichiometry. (*d*) SDS–PAGE gel stained with Coomassie Blue of fractions 10–22 from gel-filtration analysis of the CBL–SLAP2 complex. Peaks 1, 2 and 3 represent CBL–SLAP2 complex, CBL and SLAP2 degradation products, respectively. (*e*) Crystals of the CBL–SLAP2 complex.

residues (25–47 and 353–357) correspond to the unassigned density, as an insufficient number of residues exist to cover the distance between the modelled N-terminus of CBL and the N-terminus of the unassigned density. Additionally, the sequence of the missing CBL residues (^{25}IGLMKDAFQPHH HHHHHLSPHPP^{47}) does not fit the unassigned density.

To simplify the purification of SLAP2 in complex with CBL TKBD and to further define the SLAP2 binding region, we

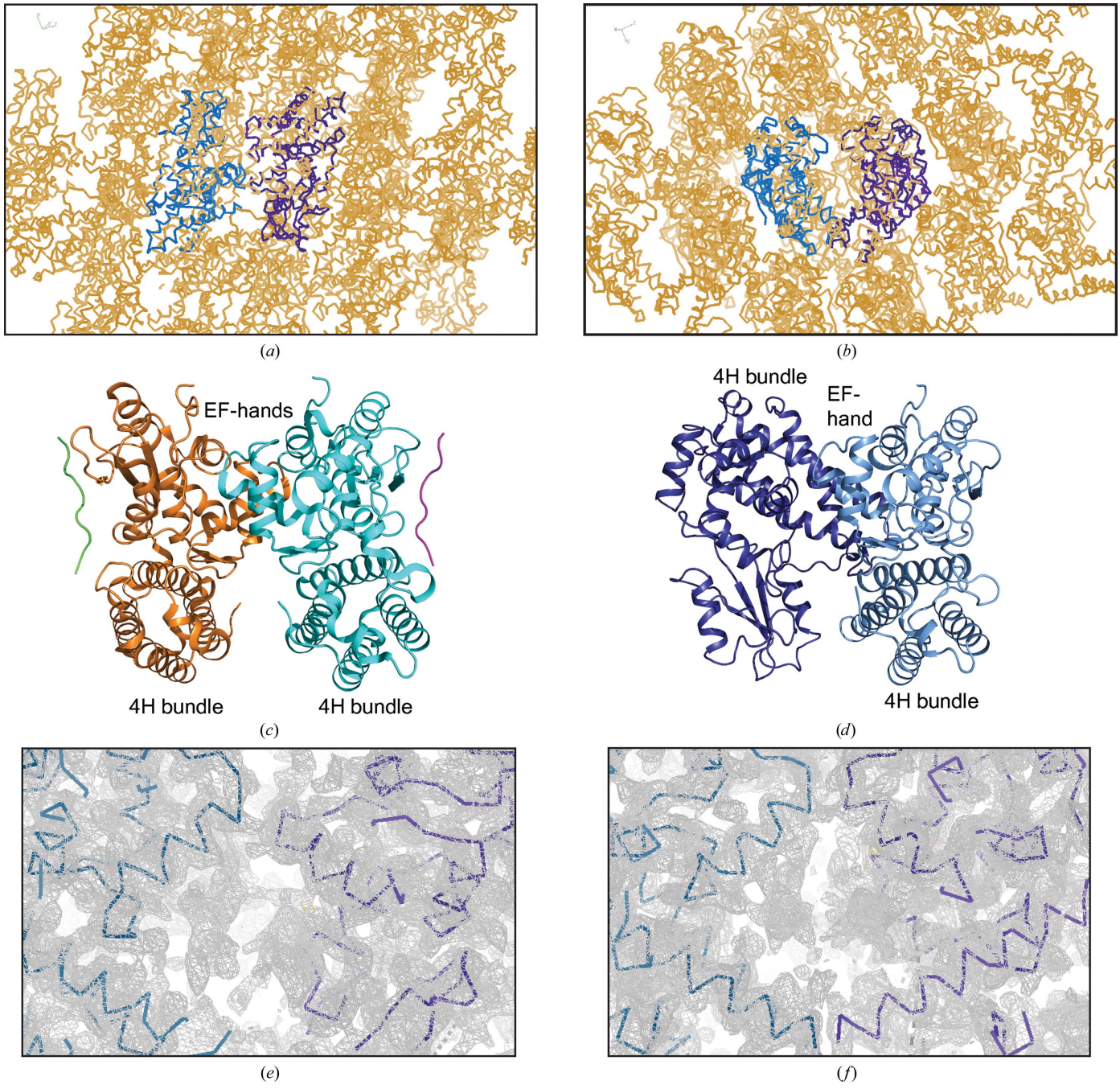

Figure 2
Distinct crystal packing of CBL TKBD monomers. (*a*) C$^{\alpha}$ traces of the CBL TKBD crystal structure, with the C$^{\alpha}$ trace of CBL molecules 1 and 2 shown as light blue and purple lines and symmetry-related molecules as calculated by *Coot* shown in orange. (*b*) As in (*a*) but with a different orientation of the dimer interface. (*c*) Ribbon representation of the C$^{\alpha}$ atoms of a representative CBL structure (PDB entry 3buw, which was chosen because it contains two CBL molecules), with molecules 1 and 2 shown in cyan and orange, respectively, pTyr peptides shown in magenta and green, and the TKBD 4H bundles labelled. (*d*) Ribbon representation of the C$^{\alpha}$ atoms of the CBL TKBD crystal structure, with molecules 1 and 2 shown in light blue and purple, respectively, and the TKBD 4H bundles labelled. Molecule 1 is in approximately the same orientation as that in (*c*). (*e*) Electron density at the CBL dimer interface is shown in grey, with the C$^{\alpha}$ trace of CBL molecules 1 and 2 shown as light blue and purple lines, respectively. (*f*) As in (*e*) but rotated approximately 90° about the horizontal axis. (*a*), (*b*), (*e*) and (*f*) were prepared with *Coot*; (*c*) and (*d*) were prepared with *PyMOL* (version 1.5.0.4; Schrödinger) Stereo versions of (*c*) and (*d*) are available as Supplementary Fig. S1.

generated a Duet co-expression vector system. The human SLAP2 sequence (residues 29–261) was preceded by thioredoxin (Trx) and His-tag fusion proteins to allow the co-purification of CBL TKBD, which bound to Trx-His-hSLAP2 during the initial Ni–NTA affinity-chromatography purification step (Fig. 3*a*). Following digestion with thrombin to remove fusion proteins and subsequent elution from the Ni–NTA resin, the CBL–SLAP2 complex was further purified by gel-filtration chromatography (Fig. 3*b*). While additional crystallization trials with this pure CBL–SLAP2 complex were unsuccessful, we observed that fractions that eluted at a higher volume and no longer contained CBL protein also appeared to contain degradation products of SLAP2. This suggested that the degradation products could no longer bind to CBL TKBD, especially since they were not present in the fractions where CBL and SLAP2 co-eluted. We reasoned that the region of SLAP2 involved in CBL binding was missing in the degradation products and determined their sequence by performing in-gel protease digestion on the corresponding gel bands (Fig. 3*b*, red boxes) and analysing the peptides by liquid-chromatography tandem mass spectrometry (LC-MS/MS). Notably, many peptides from the N-terminal portion of the SLAP2 C-terminal tail (residues 193–242) were identified (Fig. 3*c*, grey box), while no peptides from the C-terminus of the SLAP2 C-terminal tail (residues 243–261) were identified in either product (Fig. 3*c*, white box). These data suggest that SLAP2 was degraded C-terminal to residue 242 during the purification process and that this degraded protein could no longer bind CBL TKBD. This implies that at least a portion of hSLAP2 residues 243–261 are involved in binding CBL TKBD, since when this region is removed CBL binding is eliminated.

With this knowledge in hand, we purchased a synthetic 13-mer peptide representing the C-terminal tail of mSLAP2 (^{245}LSSYISLAEDPLD^{257}) for binding studies. Isothermal titration calorimetry (ITC) experiments failed to show association between purified CBL TKBD and the SLAP2 peptide (Fig. 4*a*). In contrast, phosphotyrosine peptides from the Zap70 and Lyn kinases, which bind the variant SH2 domain of CBL TKBD, bound to purified CBL TKBD in ITC experiments performed under similar conditions (Figs. 4*b* and 4*c*). This indicated that the 13-mer SLAP2 peptide is not sufficient for CBL binding, potentially because a larger region is required for binding or to adopt an α-helical conformation.

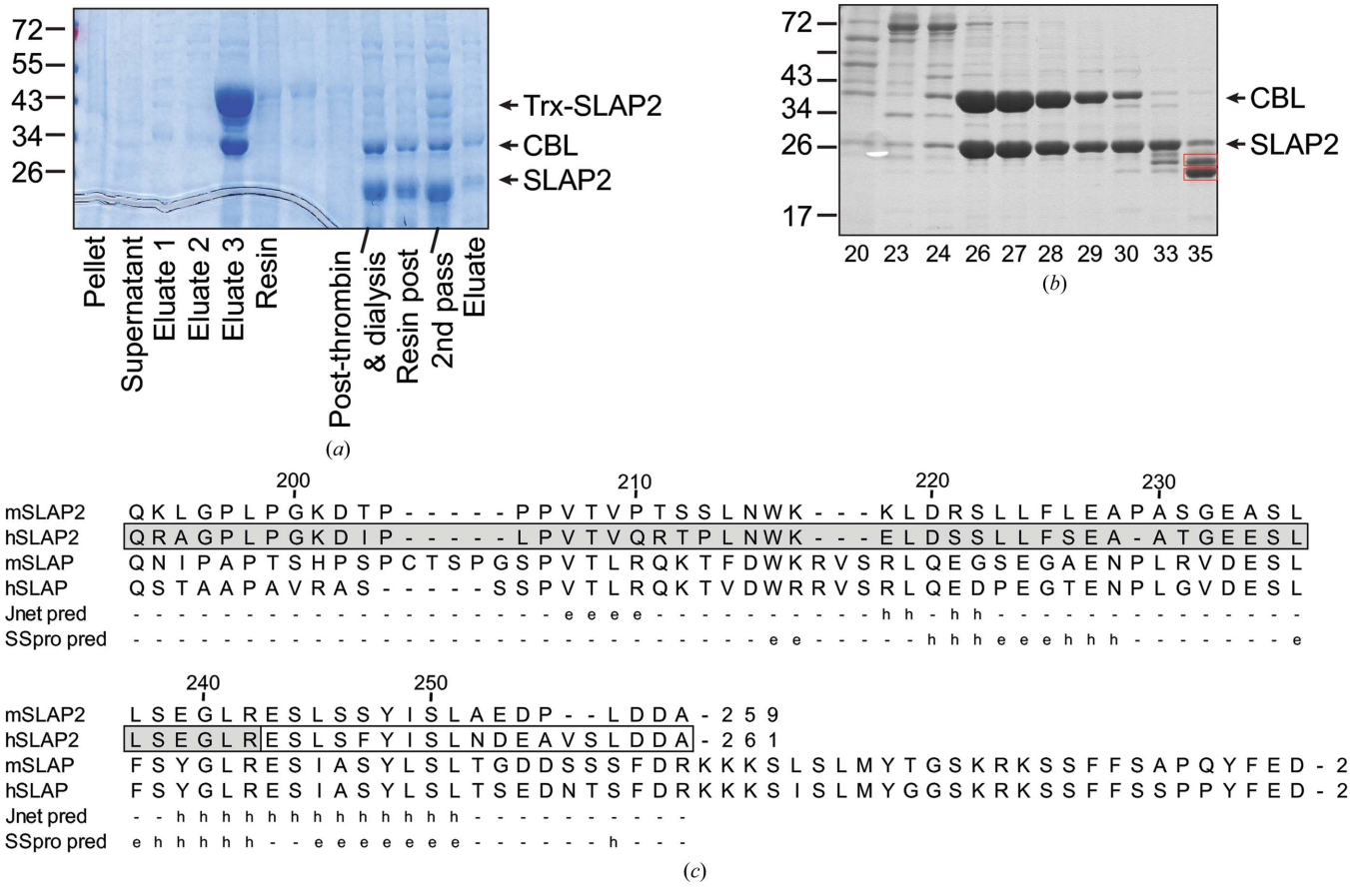

Figure 3
Co-purification of CBL–SLAP2 and mass analysis of degradation products. (*a*) SDS–PAGE gel stained with Coomassie Blue of samples from stages of CBL–SLAP2 protein co-purification. (*b*) As in (*a*) for fractions 20–35 from gel-filtration analysis of the CBL–SLAP2 complex. Red boxes indicate bands that were excised for in-gel digestion and LC-MS/MS analysis. (*c*) Sequence alignment of the C-terminal tail region of SLAP/SLAP2 proteins, with residue numbering based on human SLAP2. Secondary-structure predictions for mSLAP2 as calculated by *Jnet* (Jnet pred) and *SCRATCH* (SSpro pred) are shown, with e, - and h representing β-strand, coil and α-helix, respectively. The grey box represents residues identified by LC-MS/MS analysis. The white box represents residues that were not found in LC-MS/MS experiments.

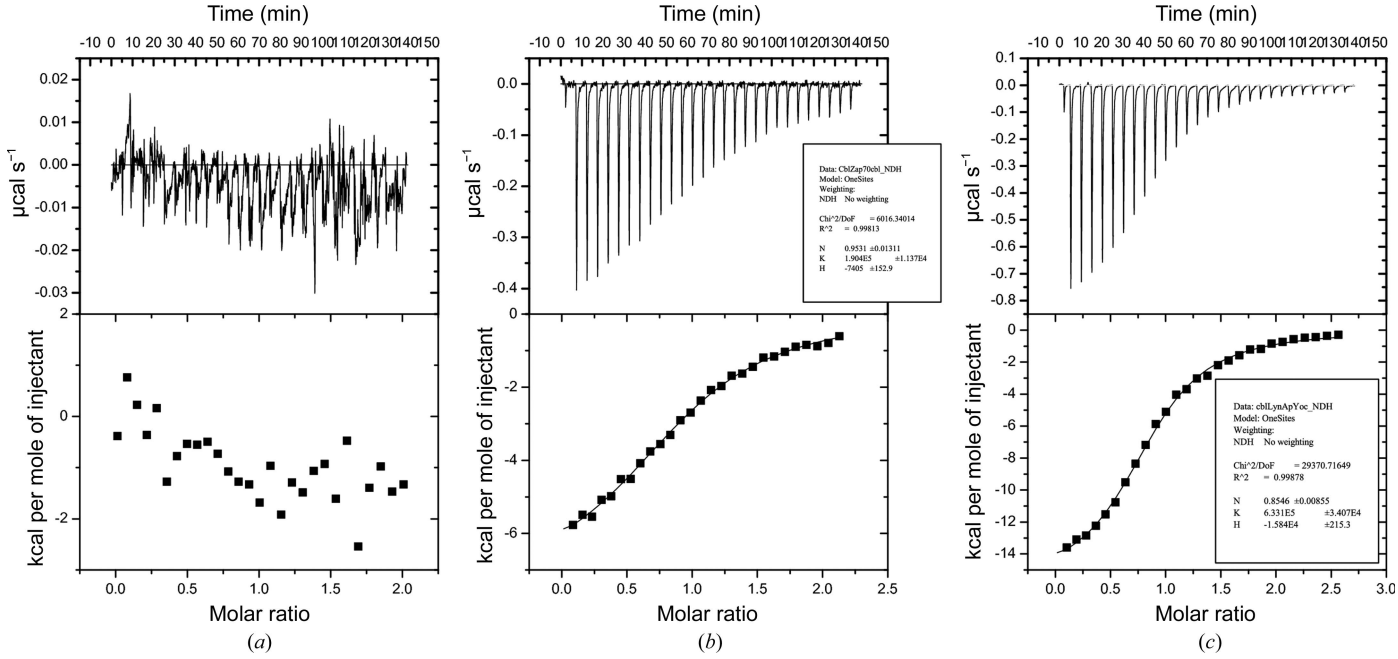

Figure 4
Isothermal titration calorimetry (ITC) data for CBL TKBD and peptides. ITC data for CBL TKBD with (*a*) mSLAP2 peptide, (*b*) Zap70-pY peptide and (*c*) Lyn-pY peptide. The top panels show the heat evolved upon injection of peptide into CBL protein plotted as a function of time. Peaks correspond to individual injections. The bottom panels show normalized integrated heats of reaction plotted against the molar ratio of total ligand concentration to total protein concentration. The solid line represents the best fit to the data according to a one-site binding model.

Large portions of the C-terminal tail of SLAP2 are expected to be disordered by secondary-structure and disorder-prediction programs (Fig. 3*c*; Drozdetskiy *et al.*, 2015; Cheng *et al.*, 2005). Knowing that disordered regions can hinder crystallization and structure determination, we sought to better understand the minimal region of SLAP2 required for interaction with CBL. To this end, we generated truncation constructs in our Duet co-expression vector and tested their ability to co-purify CBL TKBD. Residues 198–229 and/or 255–261 were deleted from the human SLAP2 C-terminal tail based on sequence conservation and predictions. Deletion of these C-terminal regions did not disrupt the co-purification of CBL TKBD (Fig. 5). This defined the region that is critical for CBL binding as residues 230–254 of hSLAP2. This is consistent with mass-spectrometric analysis of the SLAP2 degradation products and secondary-structure prediction programs, which predict either an α-helical structure or a combination of α-helical and β-strand structure in this region (Fig. 3*c*). This is also consistent with previous studies, which showed that deletion of the entire C-terminal region of SLAP2 or residues 241–261 of SLAP reduced binding to CBL *in vitro* (Holland *et al.*, 2001; Loreto *et al.*, 2002; Tang *et al.*, 1999).

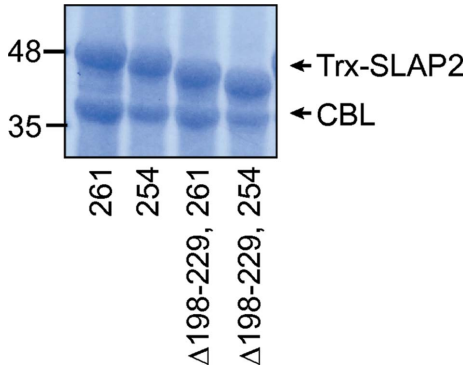

Figure 5
Co-purification of CBL–SLAP2 truncation constructs. SDS–PAGE gel stained with Coomassie Blue for CBL and SLAP2 proteins co-purified from Duet-His-Δlinker-hSLAP2-CBL 261, its truncated version Duet-His-Δlinker-hSLAP2-CBL 254, Duet-His-hSLAP2-CBL 29–261 Δ198–229 and its truncated version Duet-His-hSLAP2-CBL 29–254 Δ198–229.

Having better defined which residues of SLAP2 are both necessary for CBL binding and predicted to have secondary structure, we returned to the original CBL–SLAP2 co-crystallization X-ray diffraction data and model. Firstly, the data were integrated and scaled again at 2.5 Å resolution based on the processing statistics and limits determined by anisotropic scaling (2.5, 2.8 and 2.5 Å; Strong *et al.*, 2006). Our initial attempts at structure determination by molecular replacement employed CBL 47–351 in complex with a Zap70 phosphopeptide (PDB entry 2cbl). However, phosphopeptide binding to the CBL SH2 domain is known to induce closure of the domain, with a slight shift and rotation of the SH2 domain towards the 4H bundle (Meng *et al.*, 1999). Indeed, superposition of the C^{α} atoms of the SH2 domain of our CBL TKBD model with that of native (PDB entry 1b47) versus liganded (PDB entry 2cbl) TKBD showed greater similarity to unliganded TKBD. A subsequent attempt at MR with native CBL TKBD (PDB entry 1b47) as a model produced TFZ and LLG scores of 19.2 and 522.2, respectively, which were indicative of an improved solution. After multiple iterative cycles

of refinement with *phenix.refine* and model building in *Coot* and *Phenix* with the 'Phase and build' feature (Emsley & Cowtan, 2004; Adams *et al.*, 2010), the R_{free} was 33.0%. A feature-enhanced map (FEM; Afonine *et al.*, 2015) was calculated using *Phenix*, which further improved the quality and interpretability of the electron-density map (Figs. 6*a* and 6*b*). Polyglycine chains were placed in the unassigned density using the 'Find Helices and Strands' feature in *Phenix*, the new FEM and the improved model. Polyglycines were manually converted to polyalanines and then to mSLAP2 residues ^{240}GLRESLSSYISLAEDP^{255} in both chains of unassigned density based on the contour of the density (Fig. 6*c*). Real-space refinement in *Coot* fitted the SLAP2 residue side chains within the previously unassigned density, and refinement in *Phenix* reduced the R_{free} to 31.2%. Using a second FEM, residues ^{237}LSE^{239} were manually modelled in the last fragment of unassigned density. Final model building and refinement, and structure validation by site-directed mutagenesis experiments, are under way and the outcome will be reported shortly.

It was not possible to establish whether additional SLAP2 residues co-crystallized with CBL TKBD but remained disordered. However, based on the protein packing within the crystal (Figs. 2*a* and 2*b*) and our observation that SLAP2 is susceptible to degradation during the purification process, we conjecture that CBL–SLAP2 co-crystallized following degradation of the C-terminal tail from the SH3/SH2 domain. Based on our biochemical evidence and X-ray crystallographic data, we propose that residues 237–255 represent a significant component for CBL–SLAP2 interaction. It remains to be

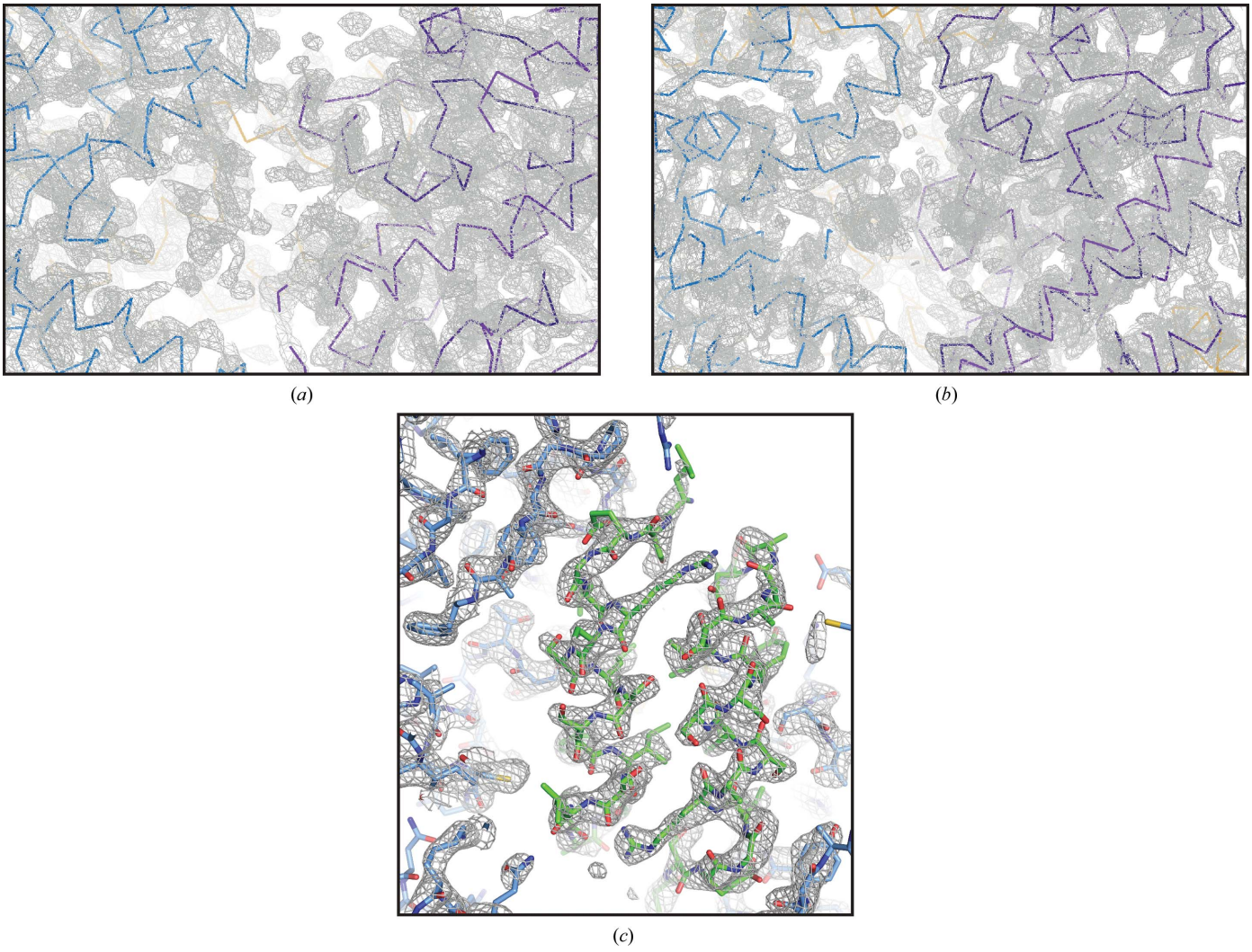

(*a*) (*b*) (*c*)

Figure 6
Modelling SLAP2 residues into unassigned α-helical electron density. (*a*) Electron density at the CBL dimer interface is shown in grey, with the C^{α} traces of CBL molecules 1 and 2 shown as light blue and purple lines, respectively. (*b*) As in (*a*) but rotated approximately 90° about the horizontal axis. (*c*) Electron density at the site of CBL and SLAP2 interaction is shown in grey, with CBL and SLAP2 atoms shown as sticks. C atoms are coloured according to their respective backbones, with CBL monomers in light blue and SLAP2 monomers in green. O and N atoms are coloured red and blue, respectively. For clarity, portions of CBL in the plane of the page have been removed. (*a*) and (*b*) were prepared with *Coot*; (*c*) was prepared with *PyMOL*. A stereo version of (*c*) is available as Supplementary Fig. S2.

determined whether the SH3/SH2 module and/or additional residues of the SLAP2 C-terminal region also associate directly with CBL TKBD.

Acknowledgements

The authors thank Savar Kaul, Julia Manalil, Alissa Visram and Mackenzie Kinney for technical assistance, Elton Zeqiraj for diffraction data collection and Frank Sicheri for access to crystallization resources and diffraction data collection.

Funding information

The following funding is acknowledged: Cancer Research Society (award to C. Jane McGlade); Garron Family Cancer Centre (award to C Jane McGlade); Canadian Institutes of Health Research (grant No. FRN166034 to C. Jane McGlade; award to Leanne E. Wybenga-Groot); American Brain Tumor Association (award to Leanne E. Wybenga-Groot).

References

Adams, P. D., Afonine, P. V., Bunkóczi, G., Chen, V. B., Davis, I. W., Echols, N., Headd, J. J., Hung, L.-W., Kapral, G. J., Grosse-Kunstleve, R. W., McCoy, A. J., Moriarty, N. W., Oeffner, R., Read, R. J., Richardson, D. C., Richardson, J. S., Terwilliger, T. C. & Zwart, P. H. (2010). *Acta Cryst.* D**66**, 213–221.

Afonine, P. V., Moriarty, N. W., Mustyakimov, M., Sobolev, O. V., Terwilliger, T. C., Turk, D., Urzhumtsev, A. & Adams, P. D. (2015). *Acta Cryst.* D**71**, 646–666.

Cheng, J., Randall, A. Z., Sweredoski, M. J. & Baldi, P. (2005). *Nucleic Acids Res.* **33**, W72–W76.

Dragone, L. L., Myers, M. D., White, C., Gadwal, S., Sosinowski, T., Gu, H. & Weiss, A. (2006). *Proc. Natl Acad. Sci. USA*, **103**, 18202–18207.

Dragone, L. L., Shaw, L. A., Myers, M. D. & Weiss, A. (2009). *Immunol. Rev.* **232**, 218–228.

Drozdetskiy, A., Cole, C., Procter, J. & Barton, G. J. (2015). *Nucleic Acids Res.* **43**, W389–W394.

Eck, M. J., Atwell, S. K., Shoelson, S. E. & Harrison, S. C. (1994). *Nature*, **368**, 764–769.

Emsley, P. & Cowtan, K. (2004). *Acta Cryst.* D**60**, 2126–2132.

Emsley, P., Lohkamp, B., Scott, W. G. & Cowtan, K. (2010). *Acta Cryst.* D**66**, 486–501.

Evans, P. R. (2011). *Acta Cryst.* D**67**, 282–292.

Gasteiger, E., Gattiker, A., Hoogland, C., Ivanyi, I., Appel, R. D. & Bairoch, A. (2003). *Nucleic Acids Res.* **31**, 3784–3788.

Holland, S. J., Liao, X. C., Mendenhall, M. K., Zhou, X., Pardo, J., Chu, P., Spencer, C., Fu, A., Sheng, N., Yu, P., Pali, E., Nagin, A., Shen, M., Yu, S., Chan, E., Wu, X., Li, C., Woisetschlager, M., Aversa, G., Kolbinger, F., Bennett, M. K., Molineaux, S., Luo, Y., Payan, D. G., Mancebo, H. S. & Wu, J. (2001). *J. Exp. Med.* **194**, 1263–1276.

Lebigot, I., Gardellin, P., Lefebvre, L., Beug, H., Ghysdael, J. & Quang, C. T. (2003). *Blood*, **102**, 4555–4562.

Liebschner, D., Afonine, P. V., Baker, M. L., Bunkóczi, G., Chen, V. B., Croll, T. I., Hintze, B., Hung, L.-W., Jain, S., McCoy, A. J., Moriarty, N. W., Oeffner, R. D., Poon, B. K., Prisant, M. G., Read, R. J., Richardson, J. S., Richardson, D. C., Sammito, M. D., Sobolev, O. V., Stockwell, D. H., Terwilliger, T. C., Urzhumtsev, A. G., Videau, L. L., Williams, C. J. & Adams, P. D. (2019). *Acta Cryst.* D**75**, 861–877.

Loreto, M. P., Berry, D. M. & McGlade, C. J. (2002). *Mol. Cell. Biol.* **22**, 4241–4255.

Loreto, M. P. & McGlade, C. J. (2003). *Oncogene*, **22**, 266–273.

Meng, W., Sawasdikosol, S., Burakoff, S. J. & Eck, M. J. (1999). *Nature*, **398**, 84–90.

Myers, M. D., Sosinowski, T., Dragone, L. L., White, C., Band, H., Gu, H. & Weiss, A. (2006). *Nat. Immunol.* **7**, 57–66.

Naramura, M., Kole, H. K., Hu, R.-J. & Gu, H. (1998). *Proc. Natl Acad. Sci. USA*, **95**, 15547–15552.

Ng, C., Jackson, R. A., Buschdorf, J. P., Sun, Q., Guy, G. R. & Sivaraman, J. (2008). *EMBO J.***27**, 804–816.

Pakuts, B., Debonneville, C., Liontos, L. M., Loreto, M. P. & McGlade, C. J. (2007). *J. Biol. Chem.* **282**, 17953–17963.

Pandey, A., Duan, H. & Dixit, V. M. (1995). *J. Biol. Chem.* **270**, 19201–19204.

Sosinowski, T., Killeen, N. & Weiss, A. (2001). *Immunity*, **15**, 457–466.

Sosinowski, T., Pandey, A., Dixit, V. M. & Weiss, A. (2000). *J. Exp. Med.* **191**, 463–474.

Strong, M., Sawaya, M. R., Wang, S., Phillips, M., Cascio, D. & Eisenberg, D. (2006). *Proc. Natl Acad. Sci. USA*, **103**, 8060–8065.

Tang, J., Sawasdikosol, S., Chang, J.-H. & Burakoff, S. J. (1999). *Proc. Natl Acad. Sci. USA*, **96**, 9775–9780.

Winn, M. D., Ballard, C. C., Cowtan, K. D., Dodson, E. J., Emsley, P., Evans, P. R., Keegan, R. M., Krissinel, E. B., Leslie, A. G. W., McCoy, A., McNicholas, S. J., Murshudov, G. N., Pannu, N. S., Potterton, E. A., Powell, H. R., Read, R. J., Vagin, A. & Wilson, K. S. (2011). *Acta Cryst.* D**67**, 235–242.

Wybenga-Groot, L. E. & McGlade, C. J. (2013). *Cell. Signal.* **25**, 2702–2708.

Wybenga-Groot, L. E. & McGlade, C. J. (2015). *Cell. Signal.* **27**, 267–274.